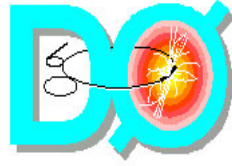


Generation of QCD Next-to-Leading Order Predictions for Comparison with DØ Results



Frederick K. Balagaddé
Manchester College
604 E. Coll. Ave., N. Manchester IN 46962

Project Supervisor: Dr. Victor Daniel Elvira
Fermi National Accelerator Laboratory*
Batavia, IL 60510
(July 28, 2000)

Abstract

The K_T algorithm has been developed as a better alternative to the cone algorithm for jet reconstruction in hadron-hadron collider experiments. The biggest advantage of the K_T over the cone algorithm is that it eliminates split/merge ambiguity. In this analysis JETRAD¹ will be used to generate next-to-leading order predictions of the inclusive jet cross-section and thrust distribution. Next-to-leading order inclusive jet cross-sections generated using the K_T and cone jet algorithms will be compared. The detector effects on measurements due to finite energy resolutions (smearing) as reflected in the inclusive jet cross-section and thrust distribution will also be addressed. From our simulations, we found that K_T jet algorithm with ($D=1$) and the cone jet algorithm with ($R=0.7$) yielded similar inclusive jet cross-sections. It was also ascertained that energy resolution smearing effects result in a systematic upward shift of the inclusive jet cross-section and population of low thrust regions of the thrust distribution.

* Operated by the Universities Research Association, under contract with the U.S. Department of Energy

¹ W.T. Giele, E.W.N. Glover, David A. Kosower, Nucl.Phys.B403:633-670,1993, [HEP-PH 9302225].

I. INTRODUCTION

The constituents of the proton - quarks and gluons - are ten thousand times smaller than the proton. In order to study the structure of the proton, a method based on the principle of the “scattering microscope²” is used. According to this method, two particles under investigation are smashed together, probing each other as deeply as possible. Detailed analysis of the debris allows the experimenter to deduce a picture of the internal structure of the collision participants. This is what takes place at the Fermilab Tevatron, where protons and antiprotons are accelerated to extremely high energies and made to collide head-on. Each hard collision converts beam particle energy into dozens of out-going particles. By placing a detector (such as the one at DØ) around the interaction point, one can measure the properties of all the particles emerging from the collision. A detailed study of their properties gives a better understanding of the proton structure. Due to the way quarks and gluons are bound inside the protons, their scattering at large angles results in the appearance of two highly energetic, collimated sprays of particles called “jets”. Examination of these jets (the direct manifestations of quarks and antiquarks) and their cross-section provides invaluable information about the underlying quark-gluon interactions.

JETRAD is a theoretical Next-to-Leading order prediction of jet cross-sections at proton-antiproton colliders. It is a simulation program that generates events one at a time, much like the experimental data collected by the DØ detector, and employs various jet algorithms to combine partons into parton-level jets.

In this paper, we shall discuss the next-to-leading order inclusive jet cross-section prediction by JETRAD. During the course of this project, JETRAD was modified to include calculations for thrust, an event shape variable, which was measured in form of thrust distributions. The smearing effects due to the detector energy resolution as reflected in the inclusive jet cross-sections and thrust distributions was also studied. Ultimately, the predictions of this investigation will be compared to the DØ experimental data, which will serve to verify the theory of strong interactions between quarks and gluons.

² The “scattering microscope” method was first demonstrated Ernest Rutherford

II. THEORY

A. Quantum Chromodynamics

According to the Standard Model, there exist six fundamental quarks and leptons as listed in the table 1. All matter is composed of a combination of these particles and their antimatter twins. For example, a proton is formed by a bound state of two up quarks and a down (uud), and a neutron is composed of two down quarks and an up (udd). Quarks primarily interact via the strong force³. They possess fractional charge categorized in three flavors labeled “color”. Each quark possesses a color charge of red or green or blue or a corresponding “anticolor” on an antiquark.

	Fundamental Particle	Symbol	Charge
Quarks	Up	u	$\frac{2}{3}$
	Down	d	$-\frac{1}{3}$
	Charm	c	$\frac{2}{3}$
	Strange	s	$-\frac{1}{3}$
	Top	t	$\frac{2}{3}$
	Bottom	b	$-\frac{1}{3}$
Leptons	Electron	e	-1
	Electron neutrino	ν_e	0
	Muon	μ^-	-1
	Muon neutrino	ν_μ	0
	Tau	τ^-	-1
	Tau neutrino	ν_τ	0

Table 1: The fundamental constituents of matter in the Standard Model.

Quantum Chromodynamics (QCD) is the theory of strong interactions between quarks mediated by gluons⁴. According to QCD, quarks are subject to the “principle of confinement,” which states that, “*the net color charge of all macroscopically observable particles must be zero.*” A proton must therefore contain a red, blue, and green quark, resulting in a net color charge of zero: [red] + [blue] + [green] = [white]. Needless to say, solitary quarks have never been observed since they each carry a single quantum of color.

³ The strong force is the strongest of the four fundamental forces of nature.

The confinement principle may be expressed mathematically in the value of the strong coupling parameter α_s , by the variance of its strength with distance. At very short distances or very large energies, the value of α_s remains small, allowing the quarks within the hadrons (protons, antiprotons and neutrons) to rattle around nearly freely. This unique feature of QCD is referred to as “*asymptotic freedom*” for quarks: at high enough energies, the coupling to the surrounding quarks and gluons may be neglected. As the distance between the quarks increases, the coupling strength increases quickly, causing the potential energy between them to rise rapidly, which confines quarks within a particle of radius $\sim 10^{-15}$ m.

B. Jets & Jet production

As previously noted, at sufficiently high energies, the partons inside the hadrons behave nearly as free particles due to asymptotic freedom. Therefore, adequately energetic protons or antiprotons can be considered as a broadened beam of loosely bound partons (quarks and gluons). High-energy hadron-hadron collisions result in the scattering of the constituent partons. QCD predicts how the final state particles evolve from the collision.

At Fermilab, protons are collided with antiprotons after counter-rotating in a superconducting ring 1Km in radius. The Fermilab Tevatron attains a center-of-mass collision energy of 1800 GeV. Typically, only two partons, one from each colliding hadron, undergo hard-scattering. The remnants of the colliding hadrons do not undergo hard-scattering, and are considered “spectator partons”. The activity due to the spectator interactions is referred to as the “underlying event”.

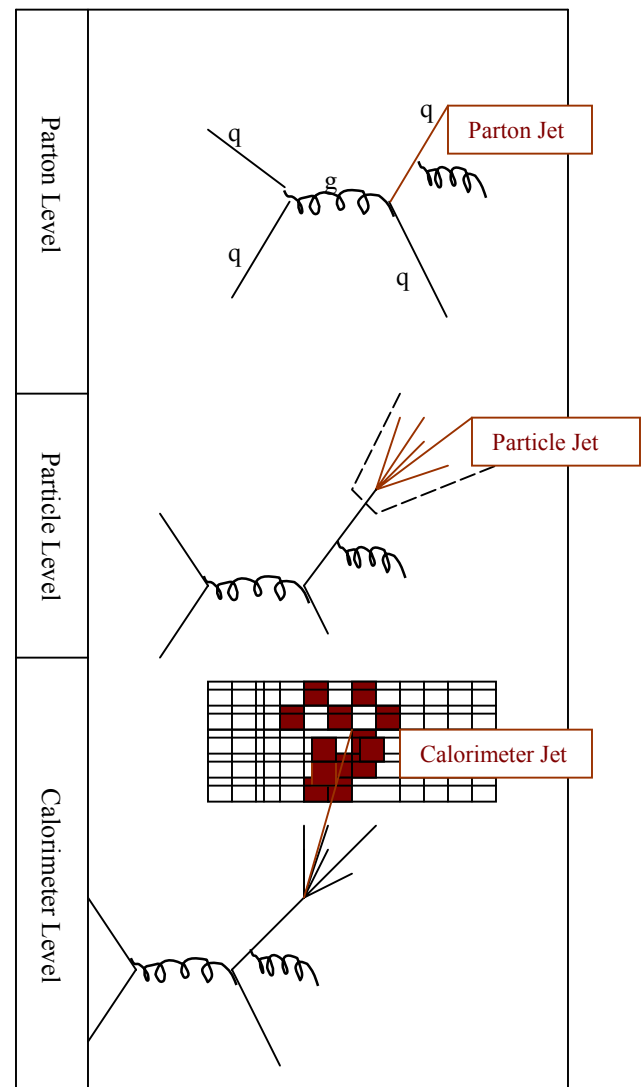


Figure 1: The three types of jets

⁴ Gluons are the strong force mediators or carriers

As the separation between the hard-scattered partons increases, the potential energy of the binding (color) force also increases and prevents the partons from escaping into isolated, colored states. At a critical point as the separation grows, the coupling constant becomes so strong that the increasing potential energy of the interaction stored in the color field tubes manifests itself by emitting gluons, which split into quark-antiquark pairs, forming a cascade or shower of elementary particles.

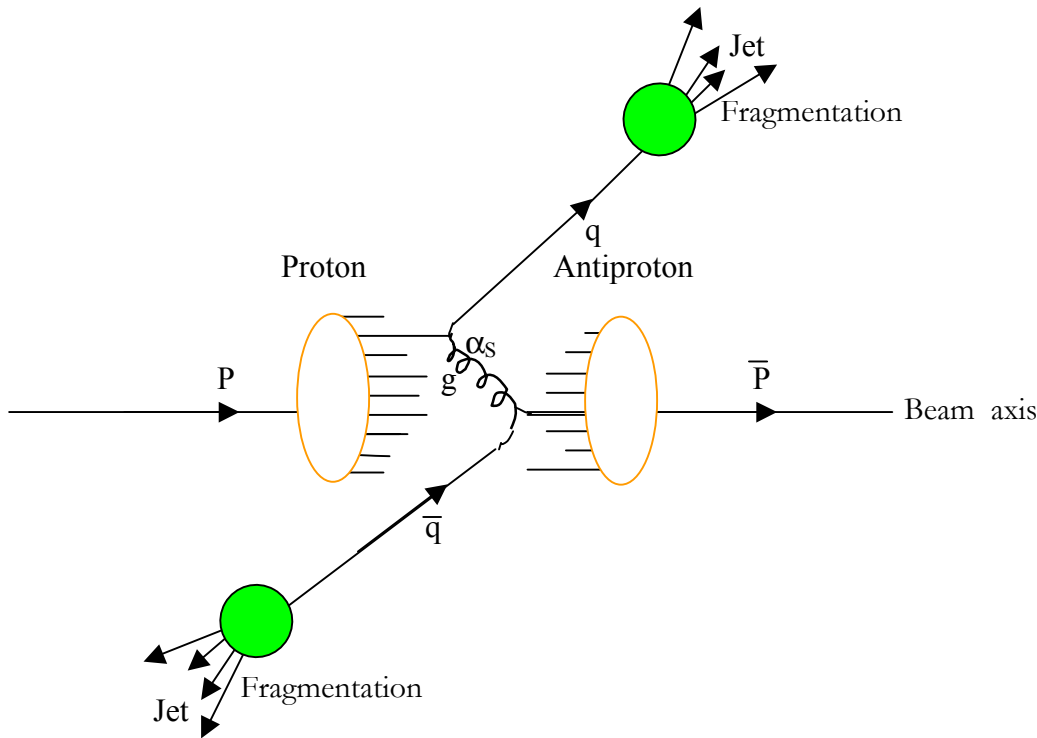


Figure 2: A cartoonist's view of jet production (Leading Order)

Partons of distinct colors in this shower then form colorless combinations, giving rise to hadrons, a process known as “dressing of the quarks”, fragmentation, or hadronization. All the partons in the shower, as well as their final products of stable, color-neutral particles gain a boost⁵ in the direction of the original partons. QCD predicts the appearance of highly

⁵ “Boost” indicates that the rest frame of the collision is not identical to the laboratory frame

collimated sprays of particles or *jets*, as evidence of the hard-scattering process in the final state. By definition, *a jet is a shower of particles emitted close to each other in angle during the hard-scattering process*. There are three kinds of jets: parton jets, particle jets, and calorimeter jets, as shown in figure 1. This analysis was restricted to jets at the parton level. The production of hadronic jets is the dominant process during hadron-hadron collisions with center-of-mass energies greater than ~ 10 GeV.

C. Parton Distribution functions

According to the parton model, a proton is made up of two up quarks and a down, which carry its flavor quantum numbers (valence quarks). It also contains other flavors of quarks and antiquarks, which form the Dirac sea (sea quarks). Sea quarks result from processes such as gluons splitting into virtual quark pairs, which almost always reabsorb.

A Parton Distribution function (PDF) describes the probability of observing a particular parton with a particular momentum in a given hadron. Each PDF is specific to the initial hadron, and contains all the information that cannot be calculated perturbatively. Such information is determined entirely by experiment. In other words, PDF's are best-fits to results of the preceding experiments. Parton momenta are integrated over all allowable values for a given hadron at a given energy, and fed into the pQCD matrix elements for the calculation of physical observables of the reactions. For example, the momentum distribution (PDF) of the valence u quark can conveniently be denoted by $u_v(x)$, where x is the fraction of the momentum of the hadron that the parton carries ($P_{\text{parton}}/P_{\text{hadron}}$). The corresponding sea distribution can be written as $u_s(x)$. The total distribution of the up quark is thus given by their sum: $u(x) = u_v(x) + u_s(x)$. The composition of the proton is thus postulated by requiring that the u_v and d_v distribution satisfy the following rules:

$$\int_0^1 dx u_v(x) = 2 \quad \text{and} \quad \int_0^1 dx d_v(x) = 1 \quad (1)$$

Various groups of physicists use different experimental methods, fitting procedures, and theoretical schemes to obtain PDF parameterizations. In this analysis, we will concentrate on PDF sets by the CTEQ⁶ collaboration: cteq3m, cteq4m and cteq4hj. The effect of using different PDF's to generate inclusive jet cross sections shall be explored.

D. The Inclusive Jet Cross-Section

The inclusive differential jet cross-section, which is sometimes denoted by $\sigma(\text{pp} \rightarrow \text{Jet} + \text{x})$, is a measure of the probability of producing a hadronic jet with a given transverse energy, E_T , during hard scattering (*cf* Appendix for definition). The term inclusive indicates that the presence or absence of additional non-jet objects in an event is not of concern. In view of the fact that the data are collected as discrete events, the analysis is performed in terms of histogram bins. The experimental formula for the inclusive double differential jet cross section is given by:

$$\left. \frac{d^2\sigma_{jet}}{d\eta dE_T} \right|_{-0.5 < \eta < 0.5} = \frac{N}{\int \mathcal{L} dt \cdot \epsilon \cdot \Delta E_T \cdot \Delta \eta} \quad (2)$$

where N is the number of events in a bin, $(\int \mathcal{L} dt)$ is the time-integrated luminosity, (ϵ) is the data selection efficiency, and ΔE_T and $\Delta \eta$ are the bin sizes in E_T and pseudorapidity, η respectively (*cf* Appendix for definitions). The instantaneous luminosity, \mathcal{L} , is associated with the number of inelastic proton-antiproton interactions per second, and the time-integrated luminosity is a measure of the total number of such events that occur during the full data collection period. The experimental determination of the inclusive jet cross-section is the most direct test of perturbative QCD. By measuring this cross-section experimentally, the structure of the proton, i.e. the PDF is better understood.

⁶ The Coordinated Theoretical-Experimental Project on QCD

E. Thrust

Thrust is an event shape variables defined as:

$$T = \max_{\mathbf{n}} \frac{\sum_i |\mathbf{P}_i \cdot \mathbf{n}|}{\sum_i |\mathbf{P}_i|} \quad (3)$$

where the sum is over all the parton or particle momenta and \mathbf{n} is the direction that maximizes T . By definition, *thrust is a measure of the “pencil-likeness” of an event.* An event with only two (back-to-back) partons or particles in the final state yields a thrust value of one. More partons or particles in the final state, i.e. more radiation, would yield a thrust value less than one. Thrust always takes values from 0.5 to unity. Transverse thrust (T_T) is defined by replacing the particle momenta in equation 3 with the momenta transverse to the beam axis to yield equation 4.

$$T_T = \max_{\mathbf{n}} \frac{\sum_i |\mathbf{P}_{Ti} \cdot \mathbf{n}|}{\sum_i |\mathbf{P}_{Ti}|} \quad (4)$$

T_T is preferred to T in a hadron collider since it is Lorentz invariant for boosts along the beam axis. The thrust definition in this analysis was modified so that only the two leading jets contributed to the thrust calculation. Thrust measurements were performed in form of thrust distributions in jet events, which were generated with JETRAD.

F. JETRAD

The inclusive jet cross-sections and thrust distributions were generated using the program JETRAD. JETRAD is a theoretical next-to-leading order event-generator for hardron-hadron colliders with numerically built-in jet algorithms, which find and reconstruct parton jets. This program is used to make predictions of observables such as inclusive jet cross-sections and thrust distributions at hadron-hadron colliders. JETRAD is a next-to-leading order prediction (α_s^3) with two or three jets in the final state as opposed to a leading order calculation (α_s^2), which would have strictly two jets in the final state. Results from

JETRAD are compared to those from experimental data to verify the theory of strong interactions between quarks and gluons.

G. The DØ Detector

The DØ detector is a large, multipurpose apparatus designed and constructed to study proton-antiproton collisions with a center-of-mass energy of up to 1800 GeV. Its name is derived from its location at the Fermilab Tevatron ring, being operated at one of the six interaction regions, identified as DØ. Its main components are: the central tracking detector, the calorimeter, and the muon spectrometer.

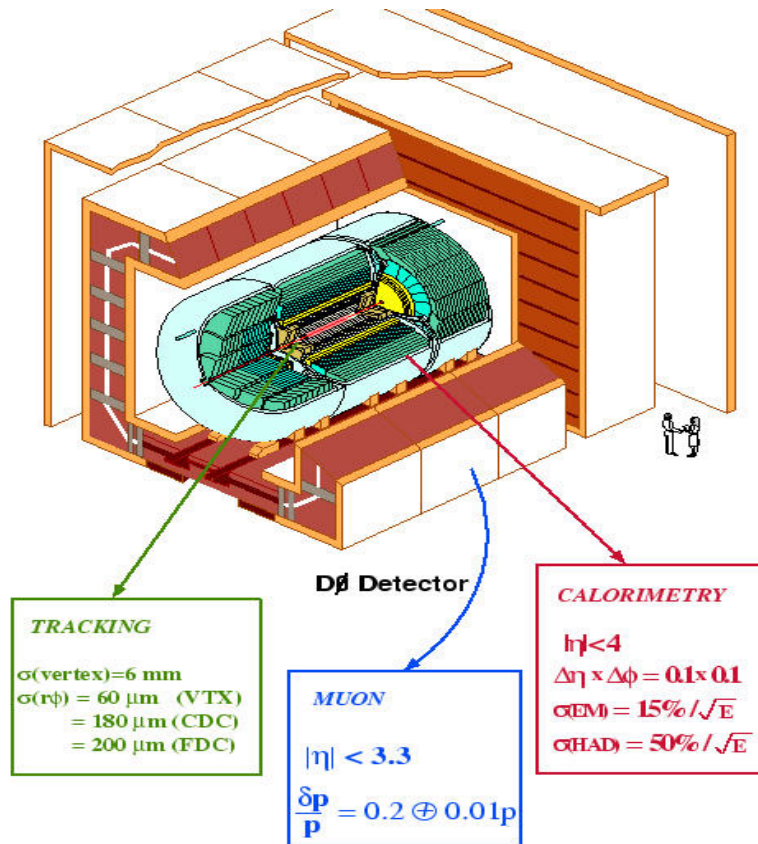


Figure 3: The DØ detector

The DØ calorimeter is the primary tool for jet measurement. This is achieved by totally absorbing the energy of the incoming particle. Upon entering the dense calorimeter

medium (Uranium), hadronic particles initiate particle cascades or showers of particles caused by secondary interactions along the path of the incident particle. The energy is deposited in detector units known as calorimeter cells. The cell centroids lie along rays of constant pseudorapidity drawn from the geometric center of the $D\emptyset$ setector. They are ganged along the rays of constant η form the $D\emptyset$ calorimeter “towers” of $\Delta\eta \times \Delta\phi$ transverse segmentation (*cf* Appendix). Each cell covers an area in $\eta \times \phi$ of $\sim 0.1 \times 0.1$ radians, providing excellent shower position resolution. The pseudoprojective nature of the $D\emptyset$ calorimeter towers is illustrated in figure 4.

Each cell unit is composed a dense absorber plate, followed by a gap of liquid argon. As a particles traverses the cell, the absorber plate serves to stop it, and the liquid argon gets ionized, creating an electric current, which is converted into voltage. This voltage is proportional to the energy of the particle.

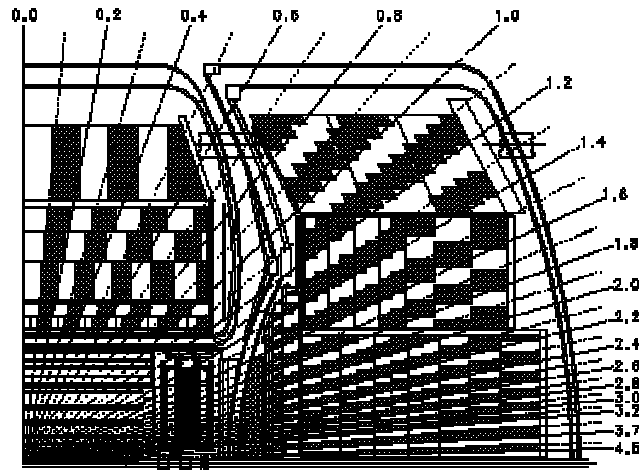


Figure 4: One-quarter η -view of the calorimeter and central detector, illustrating pseudoprojective tower geometry. Radial lines indicate detector pseudorapidity.

The calorimeter was studied and calibrated with test beams of mono-energetic particles (pions and electrons), which were aimed at different parts of the detector. The response of the calorimeter was found to be linear for energies above 10 GeV. The resolution of the pions and electron turned out to be $(0.15/[E^{1/2}])$ and $(0.5/[E^{1/2}])$ respectively (E stands for Energy).

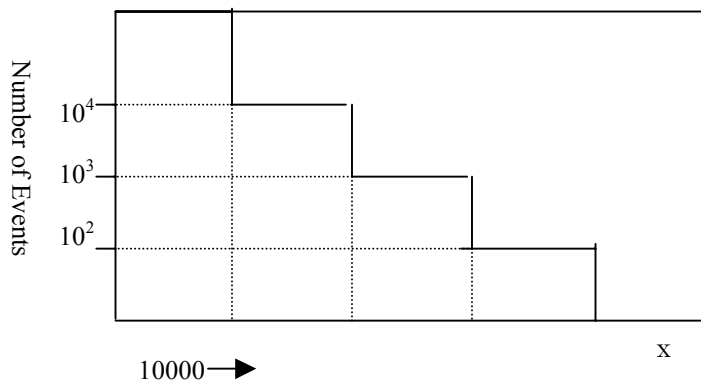
H. Instrumentation Effects

When experimental data is taken, stochastic variations in the jet energy measured result in a systematic distortion of the “true” E_T cross-section spectrum. This finite energy resolution, associated to the detector (calorimeter), produces a smearing of the jet energy spectrum, and hence the cross-section. Despite the fact that jets may be mismeasured above or below the true E_T with equal frequency, a systematic shift of the cross section occurs. This is known as the jet energy scale. Effects due to smearing become exaggerated in case of a steeply falling or rising distribution, including inclusive jet cross sections, as explained below.

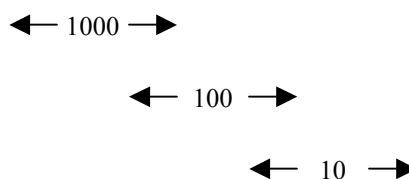
Suppose we had a steeply falling distribution measured in five bins, with the number of events in each bin determined by nature. Consider a simple case in which x is the measured quantity associated with each event. Lets assume that there is a 50% probability of over-estimating x and a 50% probability of under-estimated it, with respect to the range defined by the bin containing the true value. Lets also assume that 10% of the events migrate to the right, and another 10% to the left bin. In a scenario where the bin population decreases sharply as x becomes larger, more events migrate to the right than to the left across each boarder. Consequently, the measured distribution may be significantly larger than the one intended by nature, as illustrated in figure 5.

Smearing also causes unique transformations in thrust distributions, which we explored. As mentioned earlier, the thrust definition used in this analysis was designed such that only the two leading jets contributed to the thrust calculation. Smearing is capable of reshuffling the true E_T rankings among the parton jets of a particular event, which can decrease its “pencil-likeness” with respect to the two leading parton jets. This phenomenon is explained in figure 6.

The distribution of a variable, x , is mismeasured by more than 10%.



20% of the events in a given bin migrate across bin boundaries, 10% to the left and 10% to the right.



For a steeply falling distribution, the resulting, measured distribution is significantly larger than the true distribution (dashed)

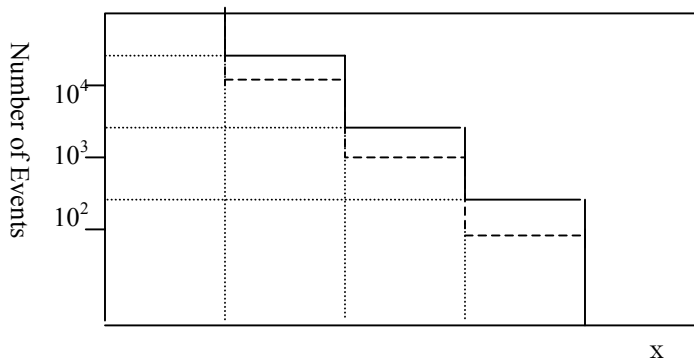
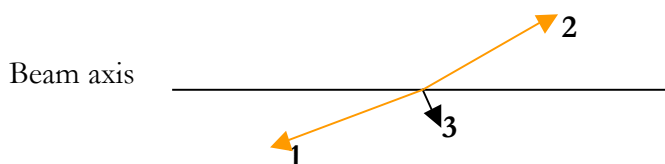
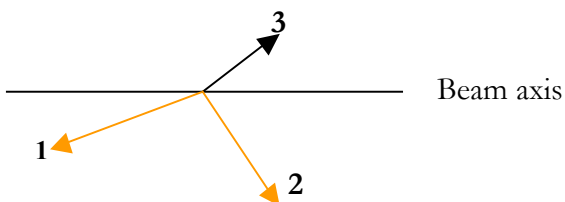


Figure 5: Illustration of the energy resolution smearing effect

Before Smearing:
“Pencil-like”



After Smearing:
Less “pencil-like”



After smearing, the new E_T ranking results in less “pencil-likeness” with respect to the two leading parton jets.

Figure 6: The effect of smearing on thrust

To incorporate energy resolution smearing effects in the inclusive jet cross-section and thrust distributions into the theory, we deliberately smeared each JETRAD event according to equation 6. The smeared predictions were compared to distributions generated from straight theory, to gain a better understanding of the gravity of the smearing effects. The fractional transverse energy resolution is expressed as $\frac{\sigma_{E_T}}{E_T}$ where σ_{E_T} is the standard deviation of the gaussian function, which describes the resolution distribution for a particle E_T . A three-parameter fit equation (equation 5) describes the fractional E_T resolution verses E_T for jets measured by the DØ detector.

$$\frac{\sigma_{E_T}}{E_T} = \left[\frac{n^2}{(E_T)^2} + \frac{s^2}{E_T} + c^2 \right]^{1/2} \quad (5)$$

In this fit n represents the contribution from uranium noise, pile-up and multiple proton-antiproton interactions (dominant at low E_T), s (sampling) describes the intermediate E_T range, and c defines the asymptotic minimum at high E_T . The parameters n , s , and c have different values depending on the η range as shown in table 2.

	Value				
Parameter	$ \eta < 0.5$	$0.5 < \eta < 1.0$	$1.0 < \eta < 1.5$	$1.5 < \eta < 2.0$	$2.0 < \eta < 4.0$
<i>n</i>	2.652	0.934	5.161	0.515	1.546
<i>s</i>	0.685	0.726	0.197	0.433	0.502
<i>c</i>	0.036	0.051	0.071	0.054	0.001

Table 2: Resolution parameters

To smear each event, the following equation is used:

$$E_{T\text{ Smeared}} = E_{T\text{ Unsmeared}} + E_{T\text{ Unsmeared}} \cdot R \cdot \left[\frac{n^2}{(E_T)^2} + \frac{s^2}{E_T} + c^2 \right]^{1/2} \quad (6)$$

III. JET RECONSTRUCTION ALGORITHMS

A jet algorithm is a selection process that associates clusters of particles (partons), which are typically emitted close to each other in angle into (finds and reconstructs) jets. It then combines their properties i.e. momentum and energy, to form the jet properties. These jet properties are related to the corresponding properties of the energetic partons produced in the hard-scattering process. In other words, jet algorithms allow us to “see” the partons or at least their evidence in the hadronic final state. Jet algorithms may be applied at the parton, particle (after hadronization) or calorimeter level (combining towers). In this analysis, we confine ourselves to jet reconstruction at the parton level.

Historically, the cone jet algorithms have been the algorithms of choice for the hadron-hadron experiments. They form jets by associating particles whose trajectories lie within an area $A = \pi R^2$ of $\eta \times \phi$ space, where η is the pseudorapidity, and ϕ is the azimuthal angle (*cf* Appendix for details on $D\phi$ coordinates and definitions).

The cone-jet algorithm starts with a trial geometric center or axis for a cone in $\eta \times \phi$ space and calculates the energy-weighted centroid, which includes contributions from all particles within the cone. As the calculation iterates, the cone center (and axis) “flows” until a “stable” solution is found i.e. until the centroid of the energy deposits within the cone coincide with the geometric axis of the cone. Figure 7 is a graphical representation of the cone jet algorithm in action. In general, working with cone algorithms can be cumbersome due to a number of factors.

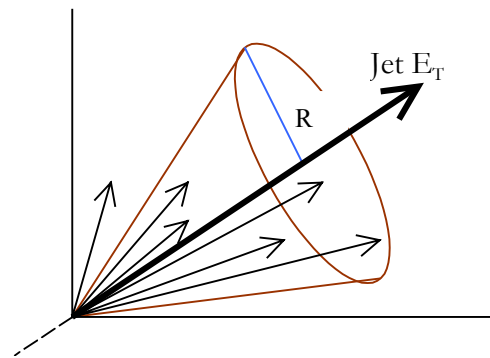


Figure 7: The cone algorithm

For example, the final stable cones might overlap, leading to the possibility of a single particle belonging to two or more cones. This problem is usually solved by including a procedure in the cone algorithm to specify how to split or merge the overlapping cones.

The K_T jet algorithm has been developed to overcome some of the theoretical difficulties involved with the cone jet algorithm. For example, it avoids out-of-bounds showering losses, therefore eliminating the split/merge obstacles. Unlike the cone jet algorithm, the K_T jet algorithm successively merges pairs of nearby particles in order of

increasing relative transverse momentum. It contains a parameter D that controls termination of merging and characterizes the approximate size of the resulting jets, as shown in equation 7.

$$d_{ij} = \min(E_{Tb}^2, E_{Tj}^2) \frac{\Delta R_{ij}^2}{D^2} \quad \& \quad d_{ii} = E_{Ti}^2 \quad (7)$$

where $R = 0.2$. Merge if $d_{ij}^2 < d_{ii}^2$ and d_{jj}^2

IV. RESULTS AND DISCUSSION

In this analysis, JETRAD was used to generate next-to-leading order inclusive jet cross sections, which were compared using the K_T and cone jet algorithms. The center-of-mass energy used for all the simulations was 1800 GeV. Figure 9 & 10 depict the spectrum of the jet cross section as defined by equation 2, integrated over the pseudorapidity range, $|\eta| < 0.5$ (the central region). The cross section decreases approximately exponentially over many orders of magnitude as shown in figure 9 & 10. In other words, the likelihood of occurrence of a jet decreases exponentially as energy increases ($\sim E_T^{-5}$).

NLO Inclusive Jet Cross-Section

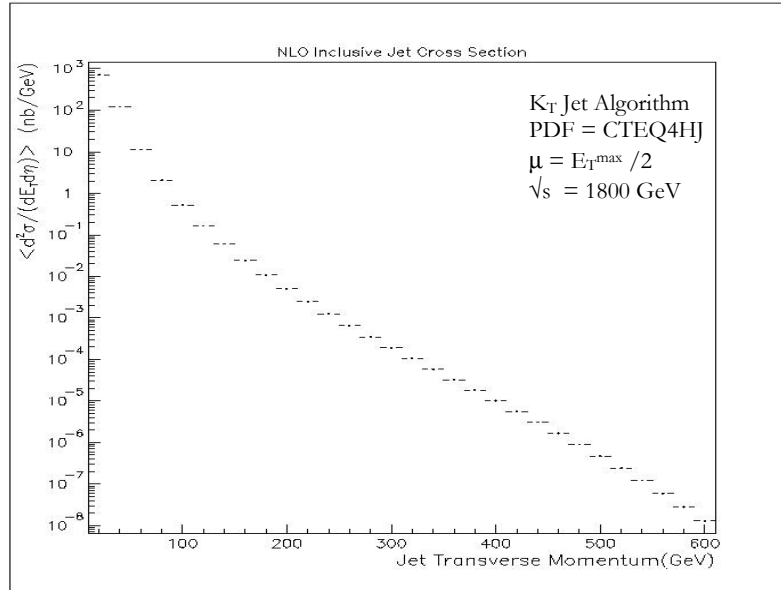


Figure 9: QCD NLO prediction for the spectrum of the inclusive jet cross-section as a function of the transverse jet momentum using the K_T algorithm

NLO Inclusive Jet Cross-Section

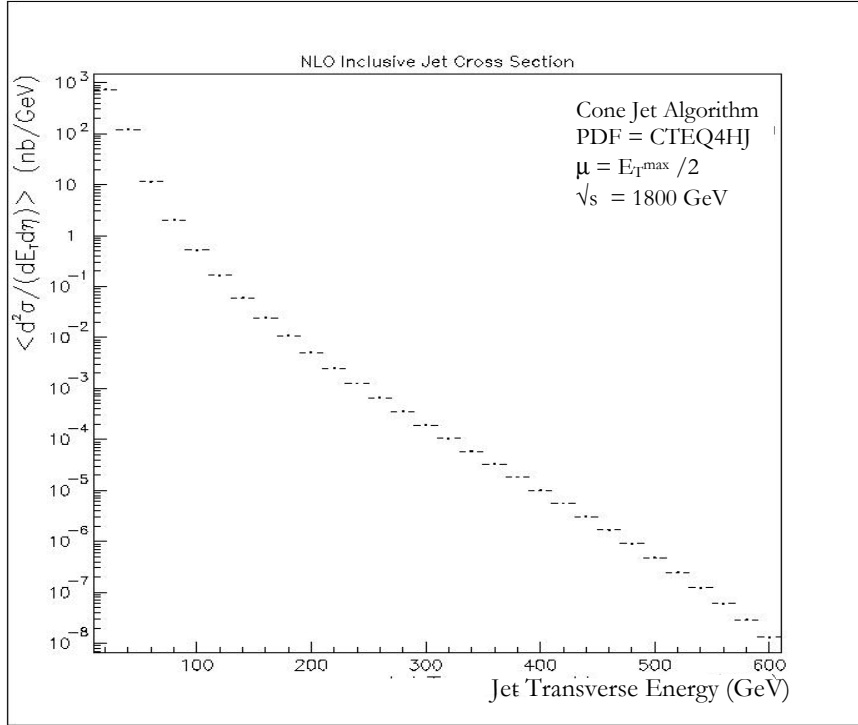


Figure 10: QCD NLO prediction for the spectrum of the inclusive jet cross-section as a function of the transverse jet momentum using the cone algorithm.

It was also ascertained that when the K_T jet algorithm was used with $D = 1$ and the cone jet algorithm with $R = 0.7$, the inclusive jet cross-section predictions about 99% similar. A quantitative comparison of both inclusive jet cross-sections made by plotting the ratio of both predictions as a function of the transverse energy is shown in figure 11.

Different choices of theoretical parameters resulted in different prediction spectra for the inclusive jet cross sections. Defining the spectrum in the figure 9 as the standard, consider the variations in the figure 12, which depict cross section differences due to different PDF's, by way of ratios. The overall uncertainty in theory due to the choice of PDF's was found to be less than 20%.

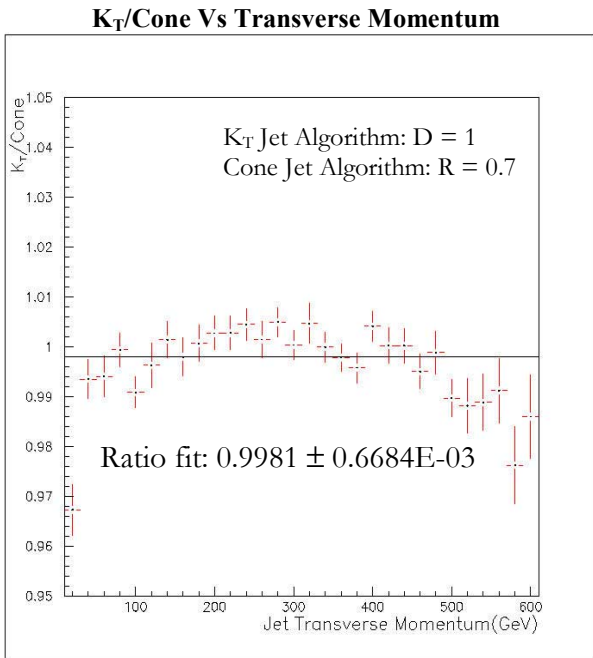


Figure 11: Comparison of the K_T & cone E_T jets
-Difference less than 1%

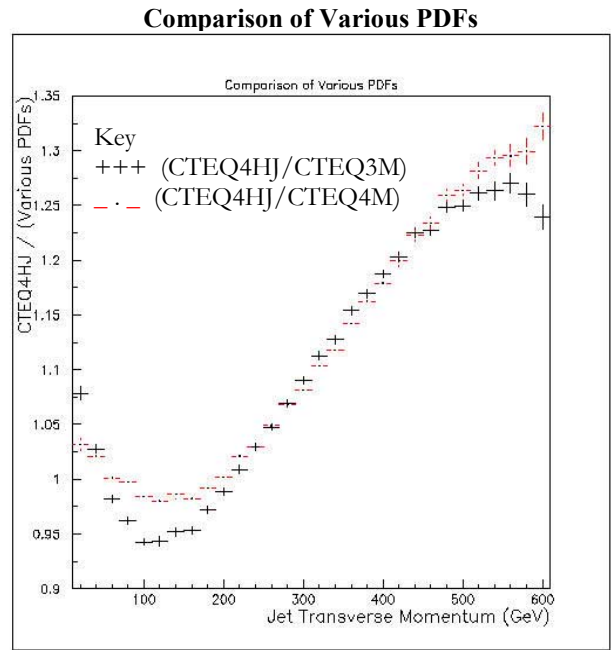


Figure 12: Comparison of cross-sections generated with various PDF's
-Overall uncertainty due to PDF choice less than 20%

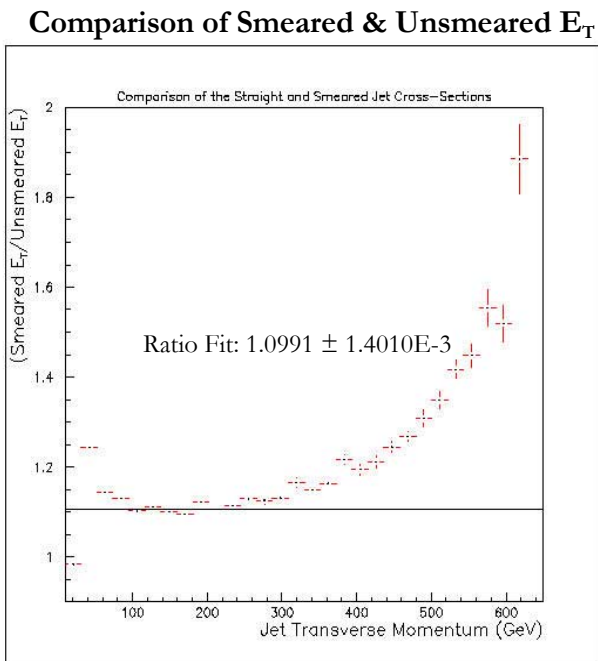


Figure 13: Comparison of cross-sections generated with straight & smeared theory
-Difference: 10%-15%

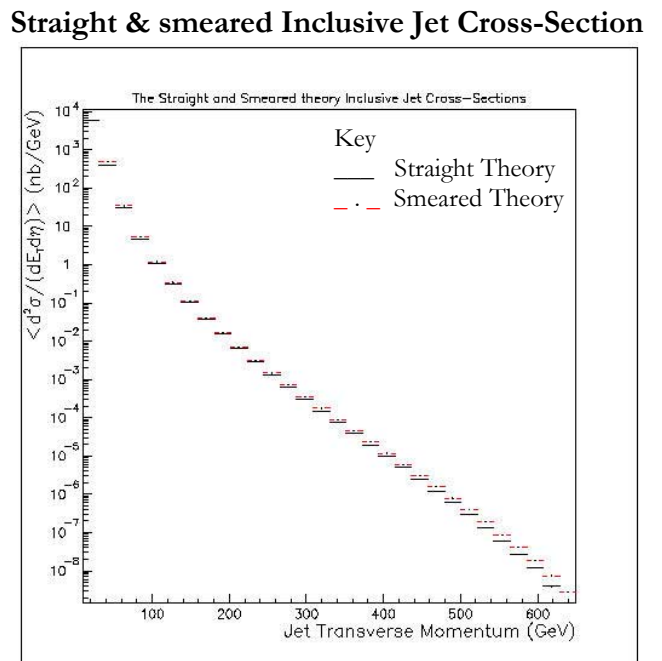


Figure 14: Differences between the smeared and straight theory NLO QCD prediction

For the inclusive jet cross section, the bin population decreases sharply with increasing E_{T_j} , therefore, more events migrated to the right than to the left across each boarder due to smearing as previously explained. This resulted in an upward shift of the inclusive jet cross-section, as illustrated in the figure 14. Figure 13 shows a quantitative comparison of the smeared and unsmeared theory by way of ratio.

As previously stated, JETRAD was also used to generate thrust distributions with the K_T algorithm for jet reconstruction algorithm at the parton level. The thrust was calculated according to equation 4, using just the two leading parton jets of each JETRAD event, integrated over the range $\eta=[-1,1]$. Figure 15 shows a T_T distribution with $H_{T3}= 90 - 150$ GeV. Evidently, the likelihood of occurrence of a jet event decreases exponentially as more radiation is emitted by the two outgoing partons. In other words, back-to-back events (Thrust = 1) occur with the highest probability.

Smearing lead to a distortion of the thrust distribution as well. Figure 16 shows the smeared thrust distribution superimposed with the straight theory distribution. The smeared distribution has more events in the lower-thrust bins than the straight theory one. The events missing in the right-most bin of the smeared theory distribution are accounted for in the lower thrust bins. There is also event migration from H_{T3} bin to H_{T3} bin.

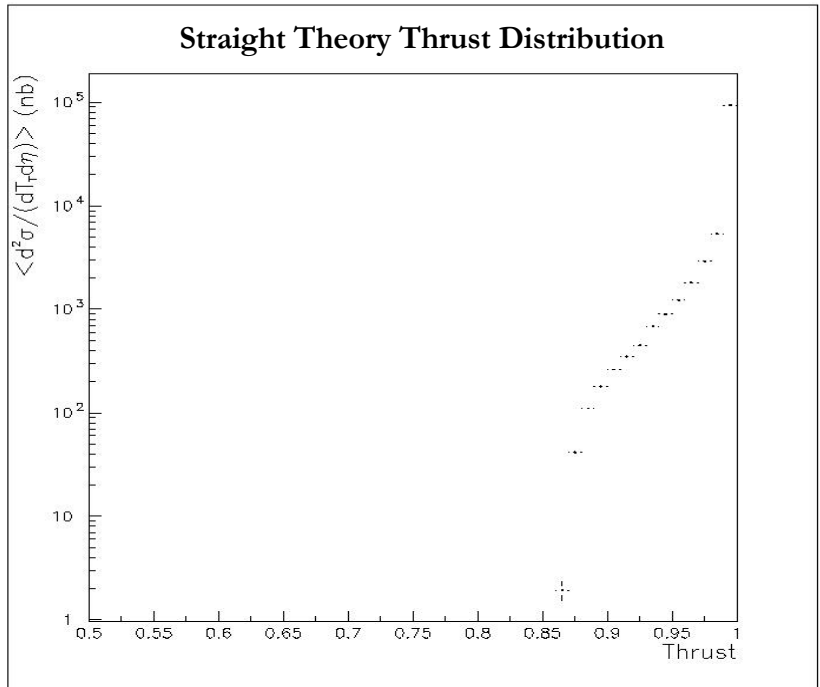


Figure 15: Thrust Distribution
-Most events are back-to-back

Smeared Theory Thrust Distribution

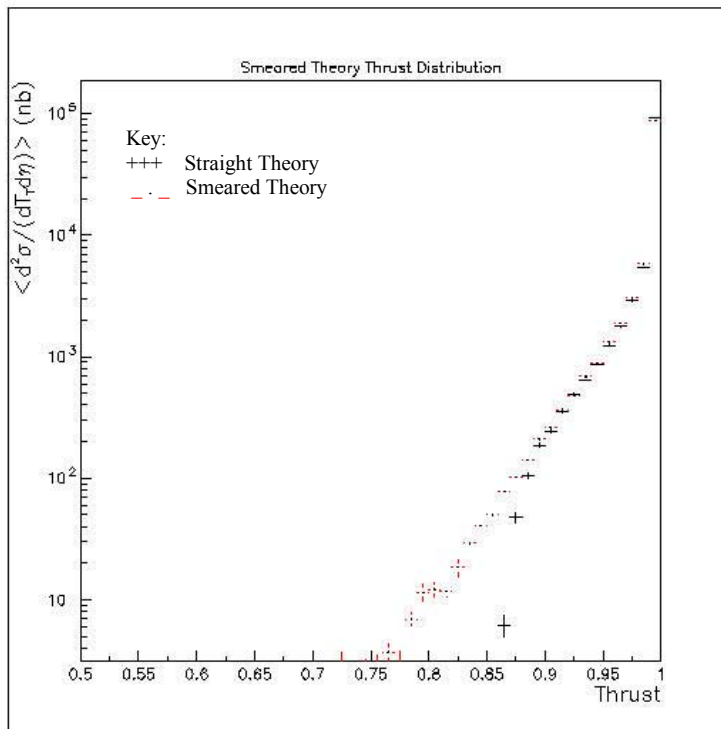


Figure 16: Smeared theory thrust distribution
 -A lot of events migrate from high to low thrust regions

V. CONCLUSION

In this analysis, our aim was to generate QCD next-to-leading order predictions for comparison with $D\bar{O}$ results. From our simulations, we found that when the K_T jet algorithm ($D=1$) and the cone jet algorithm ($R=0.7$) yielded inclusive jet cross-section predictions were 99% similar. The overall uncertainty in theory due to the choice of PDF's was found to be less than 20%. Effects like detector resolution resulted in a systematic upward shift of the inclusive jet cross-section prediction (10%-20% difference). Smearing effects led to population of the low thrust regions of the thrust distribution. Given more

⁷ H_{T3} is the scalar sum of the momentum (transverse to the beam axis) of the three leading jets of each event.

time to devote to this investigation, I would investigate the K_T prediction dependence on the parameters: D and R.

References

- [1] Run II Jet Physics 10 May, 2000
- [2] The Ratio of Inclusive Jet Cross sections by John Crane
- [3] Rapidity dependence of the single inclusive jet cross-section in proton-antiproton collisions with the DØ detector by Levan Babukhadia

Acknowledgements

I would like to thank the Summer Internships in Science and Technology committee for giving me this research opportunity. Special thanks to my project supervisor, Dr. Victor Daniel Elvira. Thank you for your invaluable advice, patience, guidance, and all the useful things you taught me about Quantum Chromodynamics. I would also like to thank Sebastian Grinstein and Sorin Maria for teaching me how to use JETRAD and Paw. The SIST program students also enriched my experience and contributed to my intellectual well-being at Fermilab.

Appendix:

Coordinate Systems, Units and Variables for HEP

The DØ collaboration uses four primary right-handed coordinate systems: Cartesian (x,y,z), Cylindrical (r, ϕ , z), spherical (r, ϕ , θ) and a modified spherical system using transverse energy, pseudorapidity, and the azimuth (E_T , η , ϕ). The fourth coordinate system defines direction and magnitude rather than the three dimensional position. The positive-z direction is always assigned to the direction of the proton beam. Thus, the x-axis points inward, toward the center of the Tevatron, and the y-axis points vertically upward. The co-latitude θ becomes zero along the z-axis, and ϕ becomes zero along the x-axis.

Natural Units

As a standard of high-energy physics, all quantities are scaled by the two fundamental constants of relativistic quantum mechanics: Planck's constant

$$\hbar = \frac{h}{2\pi} = 1.055 \times 10^{-34} \text{ J}\cdot\text{sec} \quad (8)$$

and the speed of light in vacuum

$$c = 2.998 \times 10^8 \text{ m sec}^{-1} \quad (9)$$

With the selection of units such that these quantities become dimensionless (i.e. $\hbar = c \equiv 1$), all quantities can easily be expressed in terms of energy, typically electron volts. It also follows that mass (m), momentum (mc), and energy (mc^2) all have the same units (GeV), as shown in the table below.

QUANTITY	UNITS
mass (m), momentum (mc), and energy (mc^2)	GeV
Length (\hbar/mc), time (\hbar/mc^2)	GeV ⁻¹
Charge ($\hbar c$) ^{1/2}	(dimensionless)

Table 3: Quantity units in high energy physics

As an exception to the convention, cross sections are expressed in terms of barns, where

$$1 \text{ b} = 1 \times 10^{-28} \text{ m}^2 \quad (10)$$

Variables of Collider Physics

The transverse component of the energy of a particle or group of particles, E_T , is defined as its total energy orthogonal to the beam direction. In other words,

$$E_T = E \sin\theta \quad (11)$$

This quantity is used interchangeably with P_T , the transverse momentum, for massless particles. Because the initial particles in the beam have negligible transverse momentum components, by conservation of momentum, the vector E_T sum of all the resultant objects in an event must be zero.

The rapidity is a variable frequently used to describe the behaviour of particles in inclusively measured reactions. It is defined by:

$$y \equiv \frac{1}{2} \ln \left(\frac{E + p_{\parallel}}{E - p_{\parallel}} \right) \quad (12)$$

Where E and P_{\parallel} indicate the total energy and longitudinal momentum respectively. While rapidity is not Lorentz invariant, its first derivative is; thus the shape of a rapidity distribution will not change with boost in the longitudinal direction. In the limit that $P \gg m$, the rapidity may be replaced by the pseudorapidity η in terms of $\cos\theta = (E_z/E)$ to yield equation 6. Figure 4 shows the range of η .

$$\begin{aligned} \eta &= -\ln\left(\frac{p+p_{\parallel}}{p-p_{\parallel}}\right) \\ \eta &= -\ln\left(\tan\frac{\theta}{2}\right) \end{aligned} \quad (13)$$

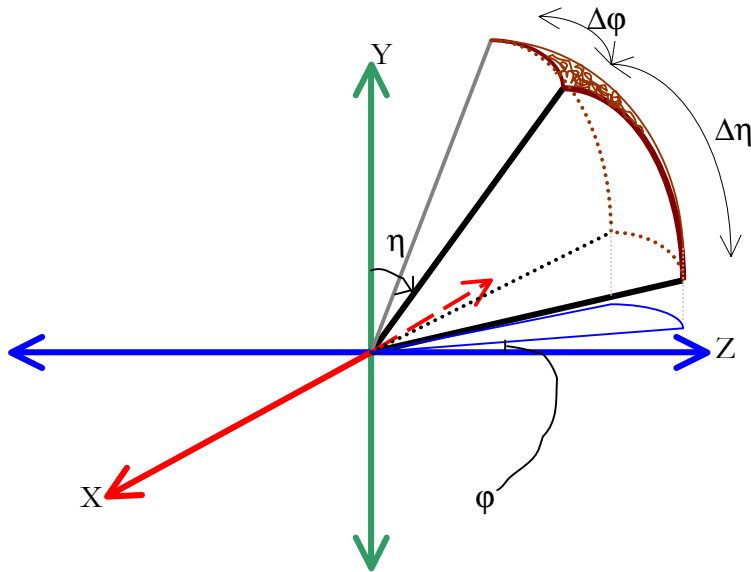


Figure 17: Graphical illustration of $\eta\chi\phi$ space